

Article

# Polysulfone/Polyamide-SiO<sub>2</sub> Composite Membrane with High Permeance for Organic Solvent Nanofiltration

Qin Liu <sup>1,2</sup>, Xing Wu <sup>1</sup> and Kaisong Zhang <sup>1,\*</sup>

<sup>1</sup> Key Laboratory of Urban Pollutant Conversion, Institute of Urban Environment, Chinese Academy of Sciences, Xiamen 361021, China; qinliu@iue.ac.cn (Q.L.); xwu@iue.ac.cn (X.W.)

<sup>2</sup> University of Chinese Academy of Sciences, Beijing 100049, China

\* Correspondence: kszhang@iue.ac.cn; Tel.: +86-592-6190782

Received: 30 August 2018; Accepted: 27 September 2018; Published: 3 October 2018



**Abstract:** To improve the filtration performance and properties of organic solvent nanofiltration (OSN) membranes, we firstly introduce nanoporous silica (SiO<sub>2</sub>) particles into the polyamide (PA) active layer of polysulfone (PSf) membrane via an interfacial polymerization process. Results from the study revealed that introduction of SiO<sub>2</sub> influenced the properties of PSf/PA-SiO<sub>2</sub> composite membranes by changing the surface roughness and hydrophilicity. Moreover, results also indicated that nanoporous SiO<sub>2</sub> modified membranes showed an improved performance of alcohols solvent permeance. The PSf/PA-SiO<sub>2</sub> composite membrane modified by 0.025 wt % of SiO<sub>2</sub> reached a permeance of 3.29 L m<sup>-2</sup> h<sup>-1</sup> bar<sup>-1</sup> for methanol and 0.42 L m<sup>-2</sup> h<sup>-1</sup> bar<sup>-1</sup> for ethanol, which were 20.0% and 13.5% higher than the control PSf membrane (permeance of 2.74 L m<sup>-2</sup> h<sup>-1</sup> bar<sup>-1</sup> for methanol and 0.37 L m<sup>-2</sup> h<sup>-1</sup> bar<sup>-1</sup> for ethanol). Conclusively, we demonstrated that the increase of membrane hydrophilicity and roughness were major factors contributing to the improved alcohols solvent permeance of the membranes.

**Keywords:** silica; polysulfone; composite membrane; polyamide

## 1. Introduction

Organic solvent nanofiltration (OSN) or solvent resistant nanofiltration (SRNF) have attracted major attention as promising technologies in the purification and separation process, especially in lube oil dewaxing [1], enhanced catalysis [2] and isolation and concentration of pharmaceuticals [3]. Compared to conventional separation processes such as distillation, evaporation, adsorption, extraction and chromatography, OSN and SRNF show several advantages including high efficiency, low energy consumption and operational stability [1].

Generally, OSN membranes could be classified as organic polymeric membranes and inorganic ceramic membranes according to the membrane materials applied for membrane fabrication [4–7]. Common polymers such as polyimide (PI) [8–11], polybenzimidazole (PBI) [12], polyetherimide (PEI) [13], polydimethylsiloxane (PDMS) [14–16], and polyacrylonitrile (PAN) [17–20] have been mostly developed in membrane fabrication processes. These membranes show good filtration performance and a high possibility of up-scaling. However, due to the high viscosity or large molecular volume of organic solvent, these membranes have relatively low permeance for organic solvent, which greatly limits the industry application of OSN membranes. It is reported that the permeance of polar organic solvents can be enhanced with the improvement of hydrophilicity for OSN membranes [21]. To date, considerable effort has been devoted to improving the hydrophilicity of conventional membranes by employing various techniques, including coating [22,23], blending [9,24,25] and surface

grafting polymerization [26]. Among these fabrication methods, blending membranes with inorganic nanoparticles such as Metal-Organic Frameworks (MOFs) [6,27,28], metals [29] or carbide [30,31] has been widely used to fabricate inorganic-organic composite membranes. Among these nanoparticles, silica (SiO<sub>2</sub>) has been proved to be a promising candidate to blend with membrane during the process of casting solution preparation [24,25], and has also shown benefits such as low cost, a simple synthesis process, high chemical stability and excellent hydrophilicity. However, blending silica with OSN membranes during the interfacial polymerization (IP) process is rarely reported [32].

As a common organic membrane material, polysulfone (PSf) has been widely used in the membrane fabrication industry. PSf-based nanofiltration membranes show excellent filtration performance, good mechanical strength and durability in water treatment [33]. Recently, researchers began to focus on the application of PSf in the OSN membranes fabrication due to the stability of PSf in alcohol organic solvents [34–37]. However, to the best of the authors' knowledge, current PSf-based OSN membranes still show a low permeance of alcohol solvents [34]. Therefore, to improve on the large-scale production of PSf-based OSN membranes in industry, it is critical to improve the properties and filtration performances of OSN membranes.

In this work, we first introduced mesoporous silica into the PSf-based nanofiltration membranes during the interfacial polymerization (IP) process. The filtration performance of the prepared OSN membranes demonstrated that SiO<sub>2</sub> obviously improved the alcohol solvents permeance of PSf/PA membranes, with a minimal decrease of the rejection performance. To further investigate the property of OSN membranes, a series of analyses, such as SEM, AFM, water contact angle and a long-term filtration test were also carried out to characterize the effect of SiO<sub>2</sub> nanoparticles on the structure and performance of the OSN membranes.

## 2. Experiment

### 2.1. Materials

Polysulfone was purchased from Solvay S.A., Shanghai, China. 1-methyl-2-pyrrolidinone (NMP, ammonium (25~28% NH<sub>3</sub>·H<sub>2</sub>O), sodium lauryl sulfate (SLS), triethylamine (TEA), hexane, methanol, and ethanol were purchased from Sinopharm Ltd., Shanghai, China. Piperazine (PIP), trimesoyl chloride (TMC) and tetraethylorthosilicate (TEOS) were purchased from Tokyo Chemical Industry Ltd., Hashimoto, Japan. Cetyl trimethyl ammonium bromide (CTAB), rose-bengal (RB), bromothymol blue (BTB), crystal violet (CV), methyl orange (MO) and (±)-Camphor-10-sulfonic acid (CSA) were purchased from Aladdin Industrial Corporation, Shanghai, China. All chemicals used were of analytical grade and were used without further purification. The water used in all experiments was distilled water.

### 2.2. Synthesis of Mesoporous Silica

Mesoporous silica was prepared as described previously [26]. Typically, 2.1 mL of 2M NaOH aqueous solution was added into 288 mL distilled water under mechanical stirring at room temperature. Then, 0.6 g CTAB was introduced into the above mixture solution. After that, the solution was heated at 80 °C until a clear solution was obtained and TEOS (3 mL) was added dropwise with vigorous stirring. The mixture reaction solution was kept stirring at 80 °C for 2 h. After reaction, the product was centrifuged, collected, and further washed with ethanol for several times to completely remove the template (CTAB), and dried in an oven at 50 °C. Finally, the mesoporous silica powder was obtained.

### 2.3. Preparation of PSf Substrates

The PSf substrates were prepared by phase inversion technique according to reported procedures [38]. Typically, the casting solution containing 16.5 wt % PSf, 0.3 wt % DI water, 0.3 wt % SLS and 82.9 wt % NMP was prepared. To fabricate a PSf substrate membrane, the casting solution was cast 200 μm thick onto a polyester nonwoven fabric, and immersed in a fresh DI water bath

immediately. The thickness of prepared PSf support was 155  $\mu\text{m}$  and was stored in  $\text{NaHSO}_3$  solution (1 wt %).

#### 2.4. Preparation of PSf/PA-SiO<sub>2</sub> Nanocomposite Membranes

PSf/PA-SiO<sub>2</sub> nanocomposite membranes were prepared on the PSf substrate by IP process. Typically, the aqueous phase was prepared by homogeneously mixing 91.3 mL of deionized water with 1.6 g of PIP, 3 g of CSA, 3 g of TEA, 0.1 g SLS, and different amounts (0.00 wt %, 0.0125 wt %, 0.025 wt %, 0.05 wt %, and 0.075 wt % based on the aqueous solution weight) of dry SiO<sub>2</sub> at room temperature. Then, the aqueous phase solution was casted on the PSf substrate membrane. After keeping for 45 s, the residual solution was removed from the PSf substrate by tissue papers. Then, the organic phase solution formed by dispersing 0.35 g of TMC in 100 mL of hexane solvent, was poured on the above wetted PSf substrate. After 20 s of IP reaction, the membrane was placed in an oven at 60 °C for 2 min for further cross linking. Finally, the membranes were stored in deionized water for further performance evaluation. According to the amounts of SiO<sub>2</sub> in the aqueous phase, the membranes were labelled as PSf/PA, PSf/PA-SiO<sub>2</sub> 0.0125%, PSf/PA-SiO<sub>2</sub> 0.025%, PSf/PA-SiO<sub>2</sub> 0.05%, PSf/PA-SiO<sub>2</sub> 0.075%.

#### 2.5. Characterization of Membranes

The morphological structures of PSf-SiO<sub>2</sub> membranes were characterized using a field emission scanning electron microscopy (S-4800, HITACHI Ltd., Tokyo, Japan) conducted with an energy dispersive X-ray (EDX) spectrometer (Oxford 6587, HITACHI Ltd., Tokyo, Japan). The hydrophilicity of the membranes was determined by measuring the water contact angles of the membrane surface with a contact angle goniometer (CMA200, KSV Instruments Ltd., Helsinki, Finland). At least 3 different locations on one membrane sample were measured to obtain an average value of the contact angles in each membrane.

The surface roughness of membranes was determined using a Dimension 3100 atomic force microscopy (AFM) device (Bruker Ltd., Billerica, MA, USA), under ambient condition, with a scanning area of  $2 \times 2 \mu\text{m}^2$ . At least 3 different spots on each membrane sample were recorded to obtain an average value. Moreover, the roughness value of the membranes was expressed as root mean-square roughness ( $R_q$ ), average roughness ( $R_a$ ) and maximum vertical distance ( $R_z$ ) between the highest and lowest point of the membrane surface. The results were showed in the supporting information (Figure S2 and Table S1).

The filtration performance of the membranes was measured using a dead-end cell (HP4750 Sterlitech Ltd., Washington, DC, USA) at a pressure of 3.5 bar achieved with nitrogen. The effective area of the membrane was 14.6 cm<sup>2</sup> and 25 mL alcohol solvent of dye at 20  $\mu\text{M}$  was charged in the cell. The solvent was magnetically stirred at 500 rpm. After 1 h filtration, permeate solvent was collected for permeance and rejection measurements.

The solvent permeance was determined according to the following Equation:

$$J = \frac{Q}{A \times \Delta P} \quad (1)$$

where  $Q$  is the permeance rate ( $\text{L h}^{-1}$ ),  $A$  is the effective filtration area ( $\text{m}^2$ ), and  $\Delta P$  is the pressure difference (bar).

In order to make a comparison between the permeance based on PSf/PA-SiO<sub>2</sub> membranes intuitively, a normalized permeance was employed in which the results were further calculated with the follow Equation:

$$\text{Normalized permeance (\%)} = \left( \frac{J_{\text{PSf-SiO}_2}}{J_{\text{PSf}}} \right) \times 100 \quad (2)$$

where  $J_{PSf-SiO_2}$  ( $L m^{-2} h^{-1} bar^{-1}$ ) is the solvent permeance of PSf/PA-SiO<sub>2</sub> membranes,  $J_{PSf}$  ( $L m^{-2} h^{-1} bar^{-1}$ ) is the solvent permeance of PSf membrane.

The rejection ( $R$ ) was evaluated using following Equation:

$$R(\%) = \left(1 - \frac{C_p}{C_f}\right) \times 100 \quad (3)$$

where  $C_p$  and  $C_f$  represent the dye concentrations of permeate and feed solution, respectively. Concentration of RB, BTB, CV, MO in the solvent were analyzed by UV 2450-vis spectrophotometer (Shimadzu, Kyoto, Japan). The solvent permeance and dye rejection were measured by at least three membrane samples and the results were average values of these measurements.

### 3. Results and Discussion

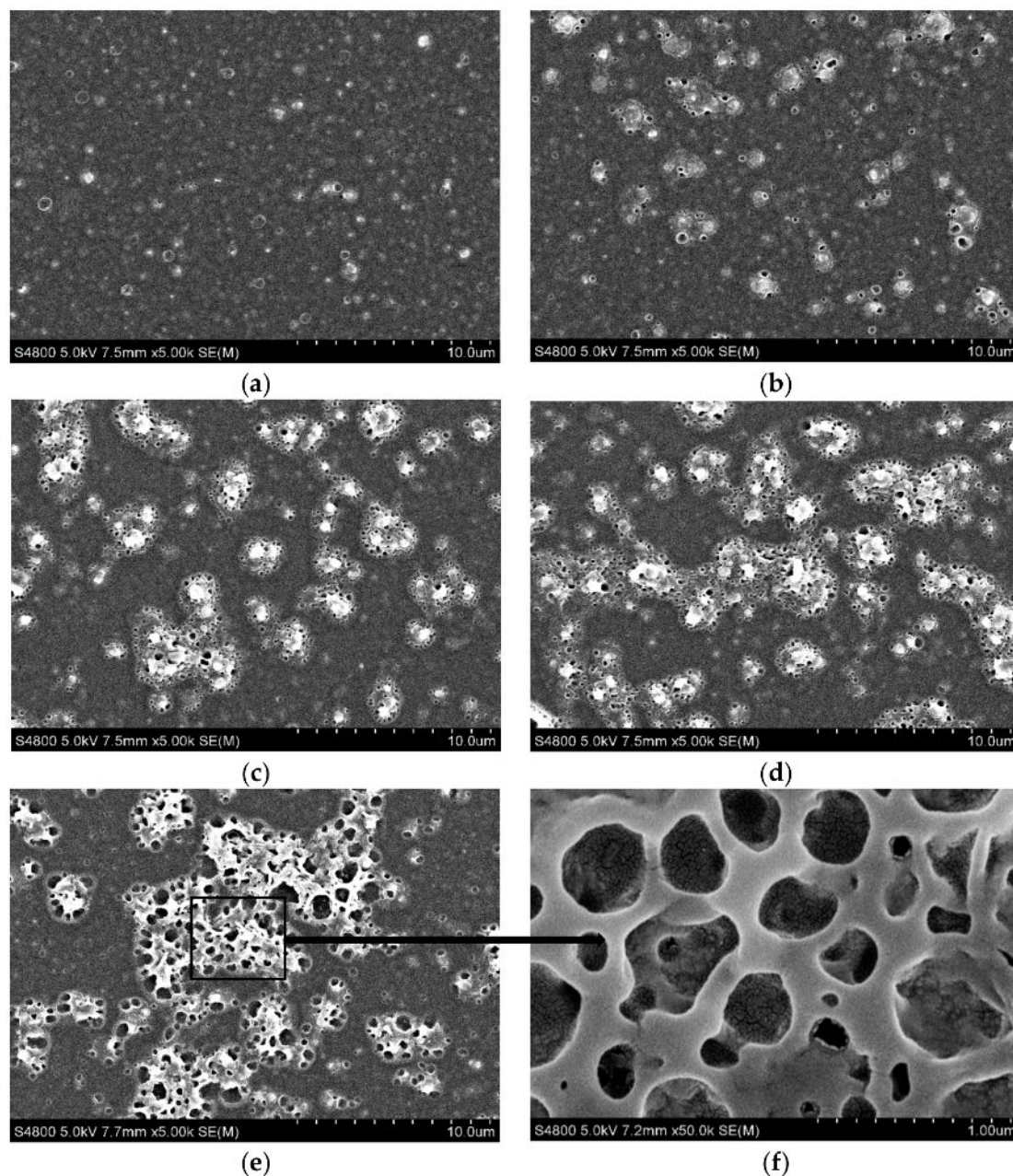
#### 3.1. Membrane Characterization

The EDX analysis of the PSf/PA-SiO<sub>2</sub> membrane and the PSf/PA membrane are given in Table 1. Only PSf/PA-SiO<sub>2</sub> membrane with 0.075 wt % SiO<sub>2</sub> and PSf/PA membrane were discussed in this section. As shown in Table 1, a new element Si with atomic ratio 0.88 appeared, while the percentage atomic ratio of O also increased, which confirmed that the SiO<sub>2</sub> nanoparticles were successfully embedded into the PA layer of PSf substrate.

**Table 1.** Atomic ratio of different element in the PSf /PA membrane and PSf/PA-SiO<sub>2</sub> membrane.

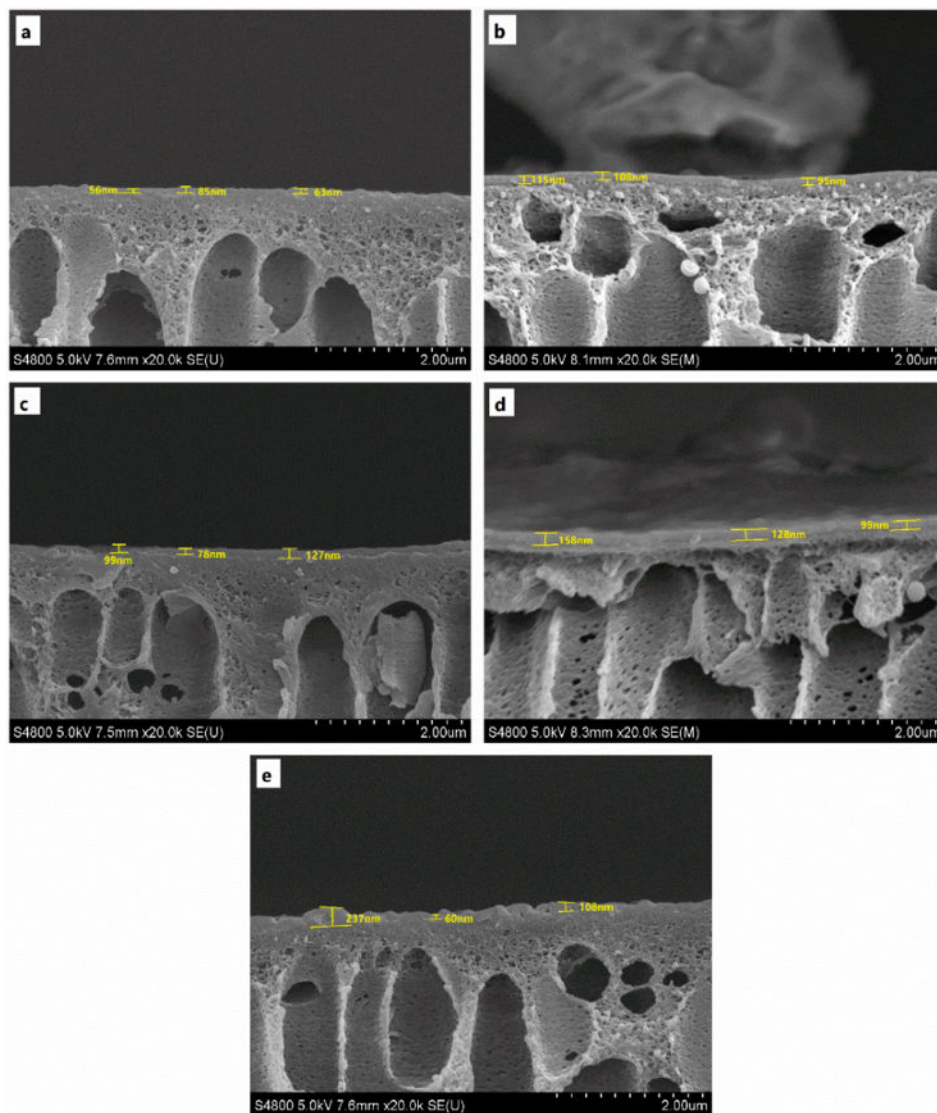
Membrane	C	O	S	Cl	N	Si
PSf/PA	72.21	20.41	4.37	0.46	2.55	-
PSf/PA-SiO <sub>2</sub> 0.075%	69.18	21.30	3.36	0.51	4.77	0.88

SEM images of the PSf/PA membrane with different amounts of SiO<sub>2</sub> are shown in Figure 1. Compared to the uniform and smooth morphological surface of PSf/PA membrane (Figure 1a), there are some bulges on the surface of SiO<sub>2</sub> doped membranes due to the embedding of SiO<sub>2</sub> nanoparticles, which make the surfaces rougher. The amount of bulges increased with the increase of the doped SiO<sub>2</sub> concentration. A similar mechanism was observed for carbon dots nanoparticles introduced into the PA layer of PSf substrate, as demonstrated in our previous work [31]. Furthermore, after the increased addition of SiO<sub>2</sub>, some showerheads-like structure appeared on the bulges, and the size of the voids in the showerhead-like structure increased with the increased concentration of SiO<sub>2</sub> nanoparticles. The introduction of the SiO<sub>2</sub> nanoparticles into PA layer during IP process can influence the formation of PA dense layer considerably, thus allowing the hydrophilic nanoparticles to adsorb onto PIP monomers, which then forms the active centers for the polymerization of PIP and TMC. This interaction makes the surface of the modified membranes different from the unmodified or control PSf/PA membrane. In order to obtain more information of the surface structure of PSf/PA-SiO<sub>2</sub>, an enlarged picture was taken (Figure 1f). It can be observed in Figure 1f that the structure of the showerhead-like bulges are not pores but the sinking of the membrane surface. In other words, the appearance of the membrane sinks or concaves will result in a rougher and higher surface area for the PSf/PA-SiO<sub>2</sub> membranes. The increase of roughness of PSf/PA-SiO<sub>2</sub> membranes can be seen clearly from the support information (Figure S1), and the AFM results in supporting information (Figure S2, Table S1) just applied to confirm this change. It can be deduced that the embedding of SiO<sub>2</sub> into the PA layer would lead to the increase of solvent permeance by providing greater surface area available.



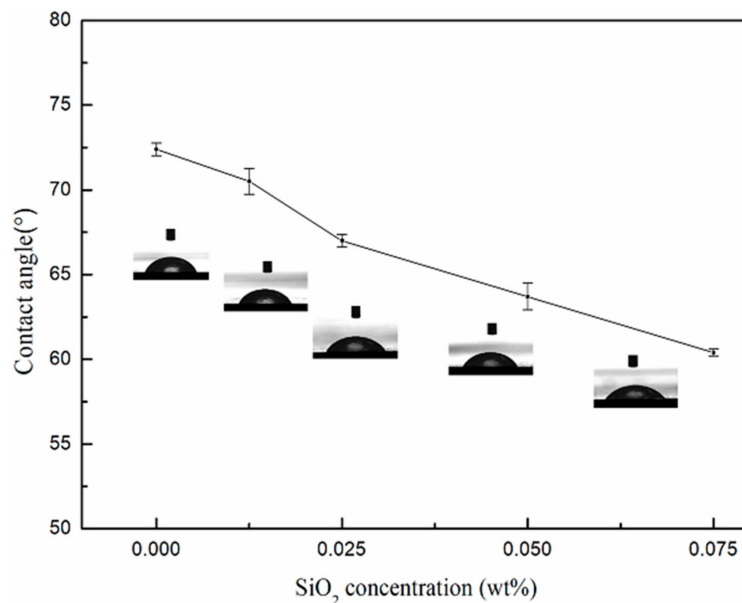
**Figure 1.** SEM pictures of surface morphology of (a) PSf/PA and PSf/PA-SiO<sub>2</sub> composite membrane with the mass fraction of SiO<sub>2</sub> of (b) 0.0125 wt %; (c) 0.025 wt %; (d) 0.05 wt %; (e) 0.075 wt % in the magnification of 5000 times; (f) the specialized area of (e) in the magnification of 50,000 times.

Figure 2 show the smooth area of cross section of the PSf/PA and PSf/PA-SiO<sub>2</sub> composite membranes, the PSf/PA membrane shows a dense PA layer and the thickness ranges from 56 nm to 85 nm. However, after the introduction of SiO<sub>2</sub>, the PSf/PA-SiO<sub>2</sub> composite membranes show a more inhomogeneity thickness and are thicker than the controlled PSf/PA membrane, particularly at high concentration of SiO<sub>2</sub>.



**Figure 2.** SEM pictures of the cross section for (a) PSf/PA and PSf/PA-SiO<sub>2</sub> composite membrane with the mass fraction of SiO<sub>2</sub> of (b) 0.0125 wt %; (c) 0.025 wt %; (d) 0.05 wt %; (e) 0.075 wt % in the magnification of 20,000 times.

The water contact angle of the membranes with different silica concentrations (0 wt %~0.075 wt %) are shown in Figure 3. The contact angle of the pure PSf/PA membrane was 72.4°. After the introduction of silica nanoparticles, the contact angle of the PSf/PA-SiO<sub>2</sub> membranes decreased from 70.5° to 60.4° with the increase of silica concentration from 0.0125 wt % to 0.075 wt %. The contact angle result indicated that the presence of SiO<sub>2</sub> in the modified membranes improved the hydrophilicity of the membrane. Two mechanisms were proposed for the improvement, these include, firstly, the abundant -OH functional groups on silica nanoparticles improved the hydrophilicity of silica nanoparticles, which subsequently increased the hydrophilicity of PSf/PA-SiO<sub>2</sub> membranes. Secondly, the influence of SiO<sub>2</sub> on the morphology of membrane surfaces is another reason to the decrease of contact angle result when SiO<sub>2</sub> was introduced into the polyamide layer of membranes. It was observed that the greater the concentration of SiO<sub>2</sub> in the polyamide layer of membranes, the rougher the membrane surface was, which consequently decreased the contact angles of membranes.



**Figure 3.** Contact angles of PSf/PA and PSf/PA-SiO<sub>2</sub> membranes.

### 3.2. Membrane Performance in Organic Solvent

#### 3.2.1. Influence of SiO<sub>2</sub> Concentration on Membrane Performance

The separation properties of the OSN membranes were investigated via filtration experiments with 20  $\mu$ M RB methanol and ethanol solutions. The influence of SiO<sub>2</sub> concentration on membrane performance was shown in Figure 4a,b. The PSf/PA-SiO<sub>2</sub> composite membranes showed improvement on the filtration performance of both methanol and ethanol solutions. Moreover, the permeance of these membranes increased with the increasing concentration of SiO<sub>2</sub> nanoparticles. As shown in Figure 4a,b, with the concentration of SiO<sub>2</sub> increased to 0.075 wt %, the permeance of methanol and ethanol increased by 38.54% and 73.84%, respectively. Meanwhile, the corresponding rejection reduced from 99.1% to 97.4%, and 98.0% to 93.8%, respectively. As a result of larger molecular volume and higher coefficient of viscosity of ethanol compared with methanol, the permeance of ethanol was lower than that of methanol. The improvement of permeance values can be a result of the improvement on hydrophilicity of the PSf/PA-SiO<sub>2</sub> membranes, which would lead to the acceleration of the penetrating rate of polar alcohol molecules. In addition, as discussed in Section 3.1, the introduction of SiO<sub>2</sub> increased the roughness of membrane surface, which is capable of increasing the effective area for permeation of alcohol molecules. Furthermore, the introduction of SiO<sub>2</sub> nanoparticles produced defective areas in the PA layer since they did not participate in the polymerization, which was the major reason for the decrease of RB rejection of the PSf/PA-SiO<sub>2</sub> membranes. However, the rejection rates of RB in the methanol and ethanol solvents are different from each other based on the same membrane, which perhaps resulted from the adsorption or physical adhesion between dye and solvents.

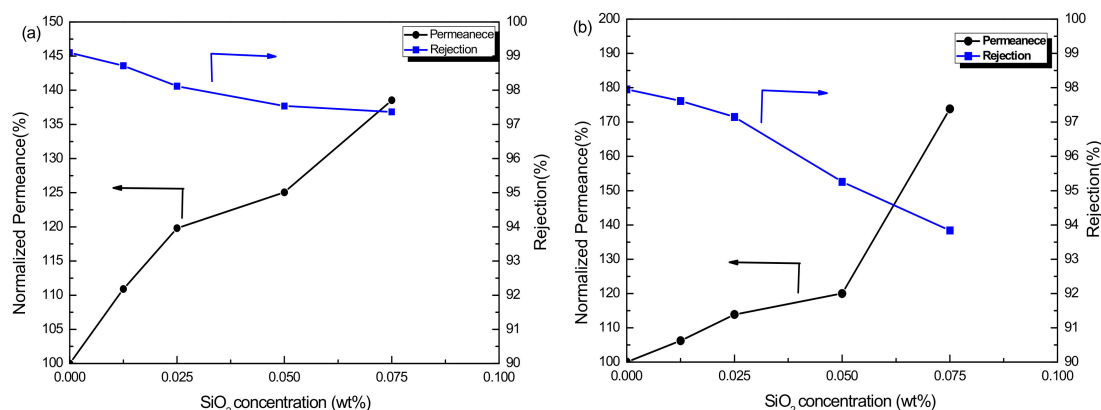


**Figure 4.** Normalized permeance and rejection of PSf/PA and PSf/PA-SiO<sub>2</sub> membranes in (a) RB/methanol solvent and (b) RB/ethanol solvent.

To further confirm the effect of SiO<sub>2</sub> concentration on the rejection performance of PSf/PA-SiO<sub>2</sub> membranes, different dyes with a concentration of 20 μM in methanol and ethanol were employed in the filtration test. The MW of these dyes was shown in Table 2. Figure 5a,b are the rejections of RB, BTB, CV and MO in methanol and ethanol respectively. It can be seen that all the rejection values of these dyes decreased with the increase of SiO<sub>2</sub> in membranes. Moreover, the reduction degrees of CV and MO were higher than that of RB and BTB. Compared to RB and BTB, CV and MO had lower molecular weights, which was the major reason for larger decreased rejections of CV and MO. The variation in trend of the rejection for these dyes in ethanol solvent (Figure 5b) was similar to the results in methanol solvent which was in the order of RB > BTB > CV > MO. Furthermore, when SiO<sub>2</sub> concentration was higher than 0.05 wt %, the rejection of PSf/PA-SiO<sub>2</sub> for MO in methanol and ethanol declined to 88.5% and 86.5% respectively, which indicated that the molecular weight cut-offs of the membranes were more than 327 Da. When SiO<sub>2</sub> concentration was higher than 0.025 wt % and lower than 0.05 wt %, the rejection of PSf/PA-SiO<sub>2</sub> for MO in ethanol was lower than 90%. Both the rejection in methanol and ethanol decreased with the increase of SiO<sub>2</sub> concentration. The above variation can be explained by the defects on the PSf/PA-SiO<sub>2</sub> membranes. The defective region of the membranes could not provide resistance to the dyes with low molecular weight. Considering the above discussion, we could infer that when SiO<sub>2</sub> concentration was 0.025 wt %, the PSf/PA-SiO<sub>2</sub> membrane display relatively excellent performance, high rejection (>90%) of MO, CV, BTB and RB both in methanol and ethanol solvent.

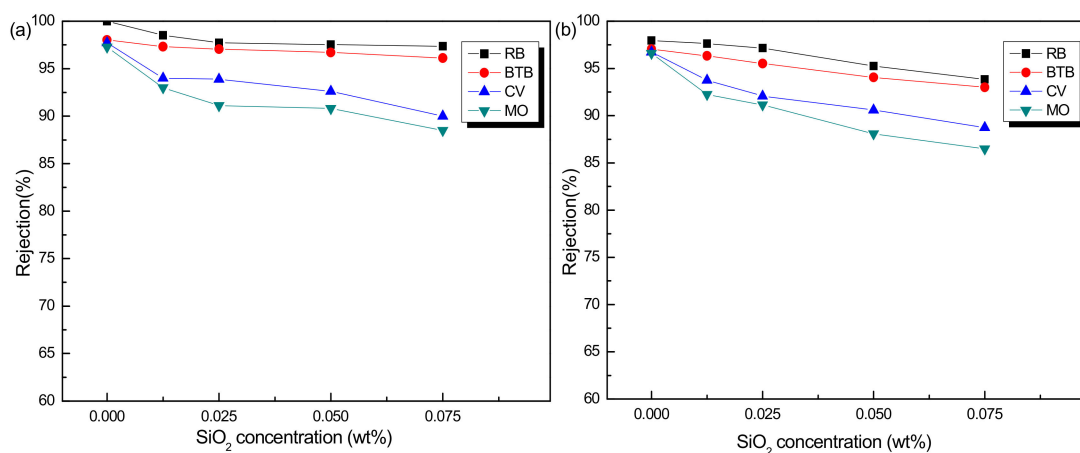


**Figure 5.** Effect of SiO<sub>2</sub> concentration on the PSf/PA-SiO<sub>2</sub> membranes, in terms of rejection for different dyes in (a) methanol solvent and (b) ethanol solvent.

**Table 2.** The molecular weight (MW) of different dyes.

Dye	RB	BTB	CV	MO
MW (Da)	1017	624	408	327

The fabricated PSf/PA-SiO<sub>2</sub> 0.025% membrane was compared with other thin film nanocomposite membranes reported in the literature. As shown in Table 3, the performance of permeance or rejection in this work is better than some reports, and the reports show both higher permeance and rejection are also difficult to be fabricated with more expensive polymer materials.

**Table 3.** Performance comparison of PSf/PA-SiO<sub>2</sub> 0.025% membrane with the other TFC membranes reported in the literature.

Membrane Type	Solvent	Permeance (L·m <sup>-2</sup> ·h <sup>-1</sup> ·bar <sup>-1</sup> )	Marker	Marker MW (g mol <sup>-1</sup> )	Rejection	Reference
PSf/PA-SiO <sub>2</sub> 0.025%	Methanol	3.29	RB	1017	98%	This work
			BTB	624	97%	
			CV	408	94%	
			MO	327	91%	
	Ethanol	0.42	RB	1017	97%	
			BTB	624	96%	
			CV	408	92%	
			MO	327	91%	
PA/PSf	Methanol	2	Bromothymol Blue	624	>90%	[34]
PA/crosslinked P84 polyimide	Methanol	1.5	Styrene oligomers	236	98%	[17]
PIM-1/polyacrylonitrile	Methanol	6	Hexaphenylbenzene	535	73%	[39]
	Ethanol	3			78%	
(PIM-1/poly(ethylene imine))/polyacrylonitrile	Methanol	3.6	Hexaphenylbenzene	535	91%	
	Ethanol	1.4			85%	
(PA/MOFs)/P84 polyimide	Methanol	3.9	styrene oligomers	236	96%	[40]
TiO <sub>2</sub> nanoparticles + PA/ polyimide	Methanol	24	Bromothymol Blue	624	>90%	[41]

### 3.2.2. Stability Performance of PSf/PA-SiO<sub>2</sub> Membrane

To further investigate the stability of the PSf/PA-SiO<sub>2</sub> membranes, the PSf/PA-SiO<sub>2</sub> 0.025% membrane with the best performance in the above study was selected and used in long period permeation tests in methanol and ethanol solvent with 20 μM RB respectively. Figure 6 shows the long-term stability of the PSf/PA-SiO<sub>2</sub> 0.025% membrane in methanol (Figure 6a), and ethanol solvent (Figure 6b). After 33 h, the membrane still showed a stable permeability and retention, confirming the excellent stability of the PSf/PA-SiO<sub>2</sub> 0.025% membrane. It is interesting that the permeance decrease of methanol was more dramatic compared to ethanol. The major reason behind this is the higher viscosity and larger molecular volume of ethanol. Overall, the prepared PSf/PA-SiO<sub>2</sub> membrane showed an outstanding separation performance for OSN application.

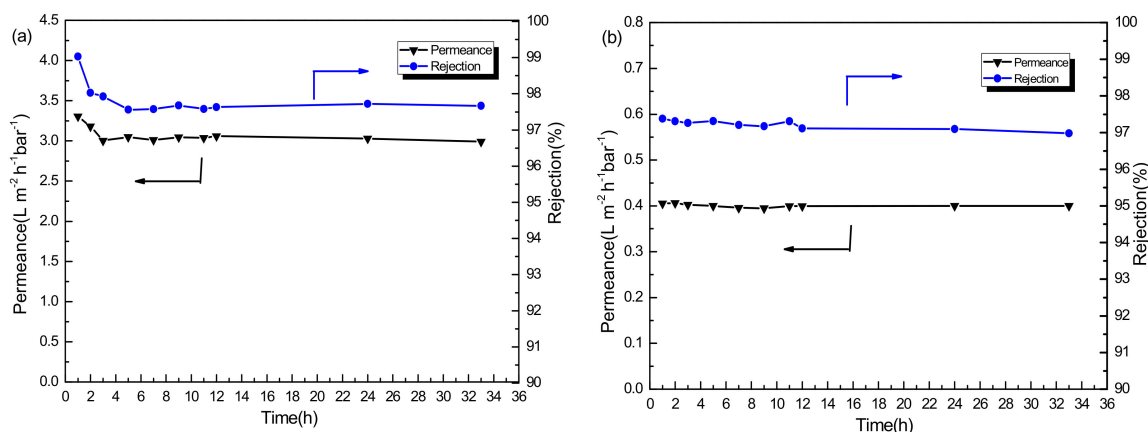


**Figure 6.** Long-time test of PSf/PA-SiO<sub>2</sub> 0.025% membrane: (a) RB in methanol solution and (b) RB in ethanol solution.

#### 4. Conclusions

PSf/PA-SiO<sub>2</sub> membranes were firstly fabricated by embedding nanoporous SiO<sub>2</sub> particles into the PA layer during the IP process, and EDX analysis confirmed the successful addition of SiO<sub>2</sub>. SEM and AFM results indicated an increase of membrane roughness after SiO<sub>2</sub> introduction. Results from a contact angle test indicated that the hydrophilicity of the membrane was improved after modification with SiO<sub>2</sub>. The performance of the OSN suggested that the permeance of methanol and ethanol for PSf/PA-SiO<sub>2</sub> membranes increased dramatically with slight decline in rejection. When the SiO<sub>2</sub> concentration was 0.025 wt %, the PSf/PA-SiO<sub>2</sub> membrane showed a relatively high rejections of RB, BTB, CV and MO dyes in methanol and ethanol solvents, which were around 90%. The long-term filtration stability test showed the excellent stability property of the newly fabricated PSf/PA-SiO<sub>2</sub> composite membrane in methanol and ethanol solvents.

**Supplementary Materials:** The following are available online at <http://www.mdpi.com/2077-0375/8/4/89/s1>, Figure S1: SEM pictures of surface morphology of (a) PSf/PA and PSf/PA-SiO<sub>2</sub> composite membrane with the mass fraction of SiO<sub>2</sub> of (b) 0.0125 wt %; (c) 0.025 wt %; (d) 0.05 wt %; (e) 0.075 wt % in the magnification of 1000 times. Figure S2: AFM 3D images of membrane PSf/PA and PSf/PA-SiO<sub>2</sub> membranes. Table S1: Surface roughness parameters of PSf/PA and PSf/PA-SiO<sub>2</sub> membranes: R<sub>q</sub>, R<sub>a</sub> and R<sub>z</sub>.

**Author Contributions:** Q.L. performed the experiments and drafted the manuscript; X.W. revised the entire article; K.Z. supervised the study and provide scientific discussions.

**Funding:** This research was funded by the Bureau of Frontier Sciences & Education, CAS (QYZDB-SSW-DQC044).

**Acknowledgments:** The authors thank the contact angle test service in Tianhe Cooperation Center for Scientific Research, the AFM test service in FUJIAN Institute of Research on the Structure, Chinese Academy of Sciences, and the greatly helpful comments from Fang Fang, Olusegun Kazeem Abass, Huali Tian, Qinliang Jiang and Bing Li. The authors are also grateful to the reviewers for their helpful and valuable comments.

**Conflicts of Interest:** The authors declare no conflict of interest.

#### References

1. Marchetti, P.; Jimenez Solomon, M.F.; Szekely, G.; Livingston, A.G. Molecular separation with organic solvent nanofiltration: A critical review. *Chem. Rev.* **2014**, *114*, 10735–10806. [[CrossRef](#)] [[PubMed](#)]
2. Vandezande, P.; Gevers, L.E.; Vankelecom, I.F. Solvent resistant nanofiltration: Separating on a molecular level. *Chem. Soc. Rev.* **2008**, *37*, 365–405. [[CrossRef](#)] [[PubMed](#)]
3. Székely, G.; Bandarra, J.; Heggie, W.; Sellergren, B.; Ferreira, F.C. Organic solvent nanofiltration: A platform for removal of genotoxins from active pharmaceutical ingredients. *J. Membr. Sci.* **2011**, *381*, 21–33. [[CrossRef](#)]
4. Huang, L.; Chen, J.; Gao, T.T.; Zhang, M.; Li, Y.R.; Dai, L.M.; Qu, L.T.; Shi, G.Q. Reduced graphene oxide membranes for ultrafast organic solvent nanofiltration. *Adv. Mater.* **2016**, *28*, 8669–8674. [[CrossRef](#)] [[PubMed](#)]
5. Xu, Y.C.; Tang, Y.P.; Liu, L.F.; Guo, Z.H.; Shao, L. Nanocomposite organic solvent nanofiltration membranes by a highly-efficient mussel-inspired co-deposition strategy. *J. Membr. Sci.* **2017**, *526*, 32–42. [[CrossRef](#)]

6. Yang, H.; Wang, N.; Wang, L.; Liu, H.X.; An, Q.F.; Ji, S. Vacuum-assisted assembly of ZIF-8@GO composite membranes on ceramic tube with enhanced organic solvent nanofiltration performance. *J. Membr. Sci.* **2018**, *545*, 158–166. [[CrossRef](#)]
7. Zeidler, S.; Puhlfürß, P.; Kätzel, U.; Voigt, I. Preparation and characterization of new low MWCO ceramic nanofiltration membranes for organic solvents. *J. Membr. Sci.* **2014**, *470*, 421–430. [[CrossRef](#)]
8. Soroko, I.; Lopes, M.P.; Livingston, A.G. The effect of membrane formation parameters on performance of polyimide membranes for organic solvent nanofiltration (OSN): Part A. effect of polymer/solvent/non-solvent system choice. *J. Membr. Sci.* **2011**, *381*, 152–162. [[CrossRef](#)]
9. Soroko, I.; Livingston, A.G. Impact of TiO<sub>2</sub>, nanoparticles on morphology and performance of crosslinked polyimide organic solvent nanofiltration (OSN) membranes. *J. Membr. Sci.* **2009**, *343*, 189–198. [[CrossRef](#)]
10. Valadez-Blanco, R.; Livingston, A.G. Solute molecular transport through polyimide asymmetric organic solvent nanofiltration (OSN) membranes and the effect of membrane-formation parameters on mass transfer. *J. Membr. Sci.* **2009**, *326*, 332–342. [[CrossRef](#)]
11. See-Toh, Y.H.; Ferreira, F.C.; Livingston, A.G. The influence of membrane formation on functional performance of organic solvent nanofiltration membranes. *Desalination* **2007**, *199*, 242–244. [[CrossRef](#)]
12. Valtcheva, I.B.; Marchetti, P.; Livingston, A.G. Crosslinked polybenzimidazole membranes for organic solvent nanofiltration (OSN): Analysis of crosslinking reaction mechanism and effects of reaction parameters. *J. Membr. Sci.* **2015**, *493*, 568–579. [[CrossRef](#)]
13. Namvar-Mahboub, M.; Pakizeh, M. Development of a novel thin film composite membrane by interfacial polymerization on polyetherimide/modified SiO<sub>2</sub>, support for organic solvent nanofiltration. *Sep. Sci. Technol.* **2013**, *119*, 35–45. [[CrossRef](#)]
14. Gevers, L.E.; Vankelecom, I.F.; Jacobs, P.A. Zeolite filled polydimethylsiloxane (PDMS) as an improved membrane for solvent-resistant nanofiltration (SRNF). *Chem. Commun.* **2005**, *19*, 2500–2502. [[CrossRef](#)] [[PubMed](#)]
15. Zeidler, S.; Kätzel, U.; Kreis, P. Systematic investigation on the influence of solutes on the separation behavior of a PDMS membrane in organic solvent nanofiltration. *J. Membr. Sci.* **2013**, *429*, 295–303. [[CrossRef](#)]
16. Li, X.; Chen, B.; Cai, W.; Wang, T.; Wu, Z.; Li, J. Highly stable PDMS–PTFPMS/PVDF OSN membranes for hexane recovery during vegetable oil production. *RSC Adv.* **2017**, *7*, 11381–11388. [[CrossRef](#)]
17. Fritsch, D.; Merten, P.; Heinrich, K.; Lazar, M.; Priske, M. High performance organic solvent nanofiltration membranes: Development and thorough testing of thin film composite membranes made of polymers of intrinsic microporosity (PIMS). *J. Membr. Sci.* **2012**, *401–402*, 222–231. [[CrossRef](#)]
18. Li, X.; Vandezande, P.; Vankelecom, I.F.J. Polypyrrole modified solvent resistant nanofiltration membranes. *J. Membr. Sci.* **2008**, *320*, 143–150. [[CrossRef](#)]
19. Li, X.; Basko, M.; Prez, F.D.; Vankelecom, I.F.J. Multifunctional membranes for solvent resistant nanofiltration and pervaporation applications based on segmented polymer networks. *J. Phys. Chem. B* **2008**, *112*, 16539–16545. [[CrossRef](#)] [[PubMed](#)]
20. Ahmadiannamini, P.; Li, X.; Goyens, W.; Joseph, N.; Meesschaert, B.; Vankelecom, I.F.J. Multilayered polyelectrolyte complex based solvent resistant nanofiltration membranes prepared from weak polyacids. *J. Membr. Sci.* **2012**, *394–395*, 98–106. [[CrossRef](#)]
21. Machado, D.R.; Hasson, D.; Semiat, R. Effect of solvent properties on permeate flow through nanofiltration membranes. Ph.D. Thesis, Technion-Israel Institute of Technology, Haifa, Israel, May 1998.
22. Sarango, L.; Paseta, L.; Navarro, M.; Zornoza, B.; Coronas, J. Controlled deposition of MOFs by dip-coating in thin film nanocomposite membranes for organic solvent nanofiltration. *J. Ind. Eng. Chem.* **2017**, *59*, 8–16. [[CrossRef](#)]
23. Altun, V.; Remigy, J.C.; Vankelecom, I.F.J. UV-cured polysulfone-based membranes: Effect of co-solvent addition and evaporation process on membrane morphology and srnf performance. *J. Membr. Sci.* **2017**, *524*, 729–737. [[CrossRef](#)]
24. Ahmad, A.L.; Majid, M.A.; Ooi, B.S. Functionalized PSf/SiO<sub>2</sub>, nanocomposite membrane for oil-in-water emulsion separation. *Desalination* **2011**, *268*, 266–269. [[CrossRef](#)]
25. Huang, J.; Zhang, K.; Wang, K.; Xie, Z.; Ladewig, B.; Wang, H. Fabrication of polyethersulfone-mesoporous silica nanocomposite ultrafiltration membranes with antifouling properties. *J. Membr. Sci.* **2012**, *423–424*, 362–370. [[CrossRef](#)]

26. Shen, L.; Feng, S.; Li, J.; Chen, J.; Li, F.; Lin, H.; Yu, G. Surface modification of polyvinylidene fluoride (PVDF) membrane via radiation grafting: Novel mechanisms underlying the interesting enhanced membrane performance. *Sci. Rep.* **2017**, *7*, 2721. [[CrossRef](#)] [[PubMed](#)]
27. Wu, X.; Shaibani, M.; Smith, S.J.; Konstas, K.; Hill, M.R.; Wang, H.; Zhang, K.; Xie, Z. Microporous carbon from fullerene impregnated porous aromatic frameworks for improving desalination performance of thin film composite forward osmosis membranes. *J. Mater. Chem. A* **2018**, *6*, 11327–11336. [[CrossRef](#)]
28. Ploegmakers, J.; Japip, S.; Nijmeijer, K. Mixed matrix membranes containing MOFs for ethylene/ethane separation Part A: membrane preparation and characterization. *J. Membr. Sci.* **2013**, *428*, 445–453. [[CrossRef](#)]
29. Liu, S.; Fang, F.; Wu, J.; Zhang, K. The anti-biofouling properties of thin-film composite nanofiltration membranes grafted with biogenic silver nanoparticles. *Desalination* **2015**, *375*, 121–128. [[CrossRef](#)]
30. Wu, X.; Field, R.W.; Wu, J.J.; Zhang, K. Polyvinylpyrrolidone modified graphene oxide as a modifier for thin film composite forward osmosis membranes. *J. Membr. Sci.* **2017**, *540*, 251–260. [[CrossRef](#)]
31. Li, Y.; Li, S.; Zhang, K. Influence of hydrophilic carbon dots on polyamide thin film nanocomposite reverse osmosis membranes. *J. Membr. Sci.* **2017**, *537*, 42–53. [[CrossRef](#)]
32. Zhang, H.; Mao, H.; Wang, J.; Ding, R.; Du, Z.; Liu, J.; Cao, S. Mineralization-inspired preparation of composite membranes with polyethyleneimine–nanoparticle hybrid active layer for solvent resistant nanofiltration. *J. Membr. Sci.* **2014**, *470*, 70–79. [[CrossRef](#)]
33. Warsinger, D.M.; Chakraborty, S.; Tow, E.W.; Plumlee, M.H.; Bellona, C.; Loutatidou, S.; Karimi, L.; Mikelonis, A.M.; Achilli, A.; Ghassemi, A.; et al. A review of polymeric membranes and processes for potable water reuse. *Prog. Polym. Sci.* **2018**, *81*, 209–237. [[CrossRef](#)] [[PubMed](#)]
34. Peyravi, M.; Rahimpour, A.; Jahanshahi, M. Thin film composite membranes with modified polysulfone supports for organic solvent nanofiltration. *J. Membr. Sci.* **2012**, *423–424*, 225–237. [[CrossRef](#)]
35. Hořda, A.K.; Aernouts, B.; Saeys, W.; Vankelecom, I.F.J. Study of polymer concentration and evaporation time as phase inversion parameters for polysulfone-based SRNF membranes. *J. Membr. Sci.* **2013**, *442*, 196–205. [[CrossRef](#)]
36. Hořda, A.K.; Vankelecom, I.F.J. Integrally skinned PSf-based SRNF-membranes prepared via phase inversion—Part A: Influence of high molecular weight additives. *J. Membr. Sci.* **2012**, *450*, 512–521. [[CrossRef](#)]
37. Struzynska-Piron, I.; Loccufier, J.; Vanmaele, L.; Vankelecom, I.; Hermans, S. Cross-linked PSf membranes for SRNF application. *Procedia Eng.* **2012**, *44*, 1348–1350. [[CrossRef](#)]
38. Liu, M.; Yu, S.; Qi, M.; Pan, Q.; Gao, C. Impact of manufacture technique on seawater desalination performance of thin-film composite polyamide-urethane reverse osmosis membranes and their spiral wound elements. *J. Membr. Sci.* **2010**, *348*, 268–276. [[CrossRef](#)]
39. Solomon, M.F.J.; Bhole, Y.; Livingston, A.G. High flux membranes for organic solvent nanofiltration (OSN)—Interfacial polymerization with solvent activation. *J. Membr. Sci.* **2012**, *423–424*, 371–382. [[CrossRef](#)]
40. Sorribas, S.; Gorgojo, P.; Téllez, C.; Coronas, J.; Livingston, A.G. High flux thin film nanocomposite membranes based on metal–organic frameworks for organic solvent nanofiltration. *J. Am. Chem. Soc.* **2013**, *135*, 15201–15208. [[CrossRef](#)] [[PubMed](#)]
41. Peyravi, M.; Jahanshahi, M.; Rahimpour, A.; Javadi, A.; Hajavi, S. Novel thin film nanocomposite membranes incorporated with functionalized TiO<sub>2</sub> nanoparticles for organic solvent nanofiltration. *Chem. Eng. J.* **2014**, *241*, 155–166. [[CrossRef](#)]

